Climatology of postsunset equatorial spread *F* over Jicamarca

Narayan P. Chapagain,[1] Bela G. Fejer,[1] and Jorge L. Chau[2]

Received 10 November 2008; revised 8 May 2009; accepted 15 May 2009; published 10 July 2009.

[1] We use radar observations from 1996 to 2006 to study the climatology of postsunset equatorial 3-m spread *F* irregularities over Jicamarca during all seasons. We show that the spread *F* onset times do not change with solar flux and that their onset heights, which occur near the altitude of the evening *F* region velocity vortex, increase linearly from about 260 to 400 km from solar minimum to solar maximum. Higher onset heights generally lead to stronger radar echoes. During the equinox, spread *F* onset occurs near vertical drift evening reversal times, while during the December solstice, they occur near the drift reversal times close to solar minimum and near the time of the prereversal velocity peak for high solar flux conditions. On average, radar plume onset occurs earlier with increasing solar flux in all seasons. Plume onset and peak altitudes increase with solar activity, and the peak heights are generally highest during the equinox. The *F* region upward drift velocities that precede spread *F* onset increase from solar minimum to solar maximum and are approximately proportional to the maximum prereversal drift peak velocities.

Citation: Chapagain, N. P., B. G. Fejer, and J. L. Chau (2009), Climatology of postsunset equatorial spread *F* over Jicamarca, *J. Geophys. Res.*, *114*, A07307, doi:10.1029/2008JA013911.

1. Introduction

[2] *F* region plasma irregularities in the nighttime equatorial ionosphere are commonly referred to as equatorial spread *F* (ESF). The occurrence of these irregularities, which have scale sizes from a few centimeters to hundreds of kilometers, varies with longitude, local time, season, and solar and geomagnetic activity. Extensive studies over the last several decades have determined the main characteristics of equatorial spread *F* [e.g., *Farley et al.*, 1970; *Woodman and LaHoz*, 1976; *Fejer and Kelley*, 1980; *Hysell*, 2000].

[3] It has been established that the height of the postsunset *F* layer is the most important parameter controlling the generation of equatorial spread *F* [e.g., *Farley et al.*, 1970; *Abdu et al.*, 1983; *Jayachandran et al.*, 1993; *Fejer et al.*, 1999]. This height is determined mainly by the equatorial vertical plasma drift velocity, which is driven by evening prereversal enhancement (PRE) of the eastward electric field. The characteristics and generation mechanisms of equatorial vertical plasma drifts have been reviewed in numerous publications [e.g., *Fejer*, 1991, 1997; *Kelley*, 1989]. The generalized Rayleigh-Taylor instability (RTI) is believed to be the mechanism responsible for the initiation of an instability at the bottomside *F* layer that develops into flux tube-aligned plasma depletions rising to the topside [e.g., *Kudeki and Bhattacharyya*, 1999; *Huba and Joyce*, 2007; *Kudeki et al.*, 2008].

[4] Extensive studies of 3-m spread *F* irregularities have been carried out since 1970 using radar observations at the Jicamarca Radio Observatory, Peru (12°S, 76.9°W, and dip latitude 1°N). *Woodman and LaHoz* [1976] presented the first detailed description of the characteristics of spread *F* scattering layers observed with the Jicamarca radar. *Hysell and Burcham* [1998] and *Hysell* [2000] studied in detail the properties of bottom-type, bottomside, and topside spread *F* observed with the 50 MHz Jicamarca JULIA (Jicamarca Unattended Long-term Investigations of the Ionosphere and Atmosphere) system. Bottom-type spread *F* events occur in relatively weak and narrow scattering layers (less than about 50 km thick) in the lower *F* region. Bottomside spread *F* events correspond to broad (about 50–100 km wide), more structured, and stronger scattering layers at relatively higher altitudes that last for a few hours. Topside layers or radar plumes represent larger-scale elongated structures originating from bottomside layers and extending to the topside ionosphere.

[5] *Kudeki and Bhattacharyya* [1999] have shown that postsunset bottomside spread *F* events commence in the interior of the *F* region evening plasma drift vortex. *Hysell and Burcham* [2002] presented a statistical study of the 3-m plasma irregularities measured by JULIA between August 1996 and April 2000 and discussed the relationship of these irregularities to the equatorial ionospheric electric fields during quiet and disturbed times. More recently, coherent scatter radar measurement over Brazil, Asia, and Micronesia have also been used to study the variability of spread *F* and its relationship to the post sunset rise of the equatorial *F* layer [e.g., *de Paula and Hysell*, 2004; *Yokoyama et al.*,

[1]Center for Atmospheric and Space Sciences, Utah State University, Logan, Utah, USA.
[2]Radio Observatorio de Jicamarca, Instituto Geofisico del Peru, Lima, Peru.

0148-0227/09/2008JA013911

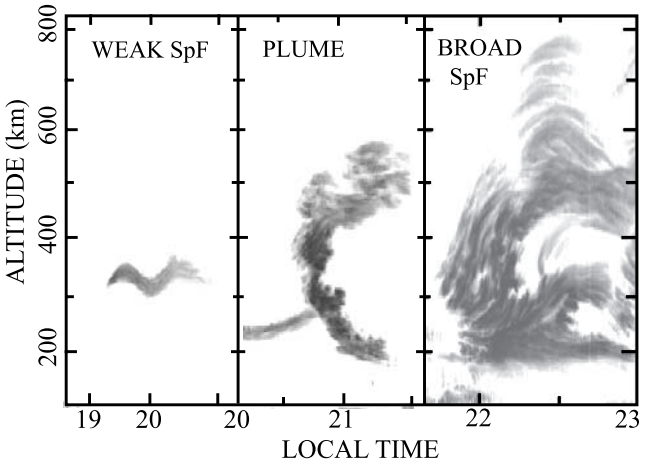

Figure 1. Range-time-intensity (RTI) plots of (left) weak spread *F* on 3 November 1999, (middle) plume on 9 September 1996, and (right) broad spread *F* on 12 September 1996, measured by the JULIA.

2004; *Patra et al.*, 2005; *Tsunoda*, 2005; *Tsunoda and Ecklund*, 2007].

[6] In this study, we use detailed coherent and incoherent radar observations to examine the climatological behavior of postsunset spread *F* over Jicamarca. This work follows up the statistical study of *Hysell and Burcham* [2002]. In the following sections, we first briefly describe our measurements and data analysis; then we will discuss the onset heights, times of initial spread *F* radar echoes and plumes, and the peak altitudes of radar plumes as well. Finally, we will highlight the relationships of spread *F* and radar plume onset times with the characteristics of the evening equatorial vertical drifts.

2. Measurements and Data Analysis

[7] We have used *F* region JULIA and incoherent scatter radar measurements over Jicamarca during 1371 evening and early night periods primarily from August 1996 to December 2006. For the June solstice, when spread *F* is less common over Jicamarca, we have also included data from 2007 and 2008. We have binned these measurements in three seasons representing equinox (March–April and September–October), December solstice (November–February), and June solstice (May–August). For each season, we classified the spread *F* structures on the basis of their thickness and range of altitudes as weak spread *F* (WSpF), plumes, and broad spread *F* (BSpF). These radar signatures are illustrated in Figure 1. WSpF is characterized by weak and narrow irregularity structures (smaller than about 150 km) with a typical value of 60 km, which corresponds mostly to the bottom-type and bottomside layers of *Hysell and Burcham* [1998]. We define radar plumes as large-scale plasma structures that break through to the topside and rapidly ascend to higher altitudes (an altitude range greater than about 200 km), and broad spread *F* as wide structured layers (thickness greater than about 200 km) with temporal scales longer than about two hours. These broad structures sometimes extend to higher altitudes and occasionally produce radar plumes. The average thickness of the broad spread *F* structure is about 350 km. We define both radar plumes and broad spread *F* as strong spread *F* (SSpF).

Table 1. Spread *F* Occurrence Over Jicamarca

	March–April, September–October		November–February		May–August	
Radar Signature	Number	%	Number	%	Number	%
No SpF	107	20	53	12	264	68
Weak SpF	166	31	194	43	73	19
Plumes	232	44	145	32	44	11
Broad SpF	25	5	61	13	7	2

[8] Over Jicamarca, postsunset spread *F* is most common during the equinox and December solstice, but only occasional during the June solstice, as illustrated in Table 1. During the equinox and December solstice most strong spread *F* events occurred during geomagnetic quiet times; during the June solstice strong spread *F* events were observed during 33 and 18 quiet and disturbed nights, respectively. *Hysell and Burcham* [2002] pointed out that the statistics of spread *F* occurrence over Jicamarca do not have significant solar cycle dependence except for a small increase in the frequency of radar plumes near solar minimum.

[9] Figure 2 highlights the main spread *F* parameters we used in the present study. These are the onset time (T_I) and height (H_I) of the initial spread *F*, and the onset time (T_P), height (H_P) and peak height (H_{PK}) of radar plumes. The plume peak heights could only be determined when the measurements covered their full altitude profiles in the RTI (Range-Time-Intensity) plots. For solar flux indices gener-

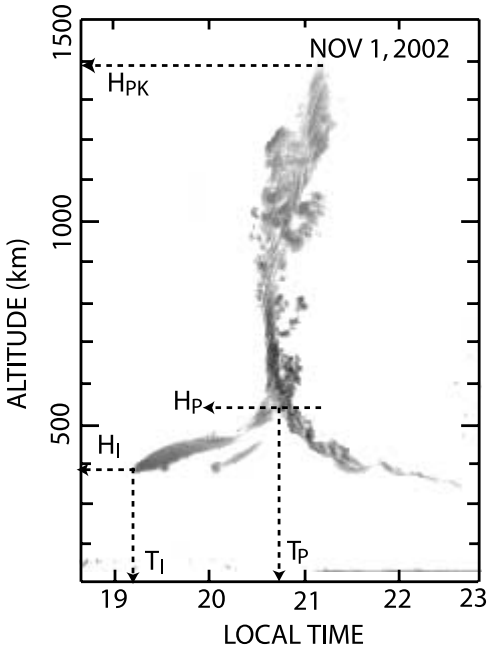

Figure 2. Typical JULIA radar plume over Jicamarca on 1 November 2002, illustrating the spread *F* parameters considered in this study. T_I and H_I correspond to spread *F* onset time and height, and T_p, H_p, and H_{pk} are the plume onset time, height, and peak height, respectively.

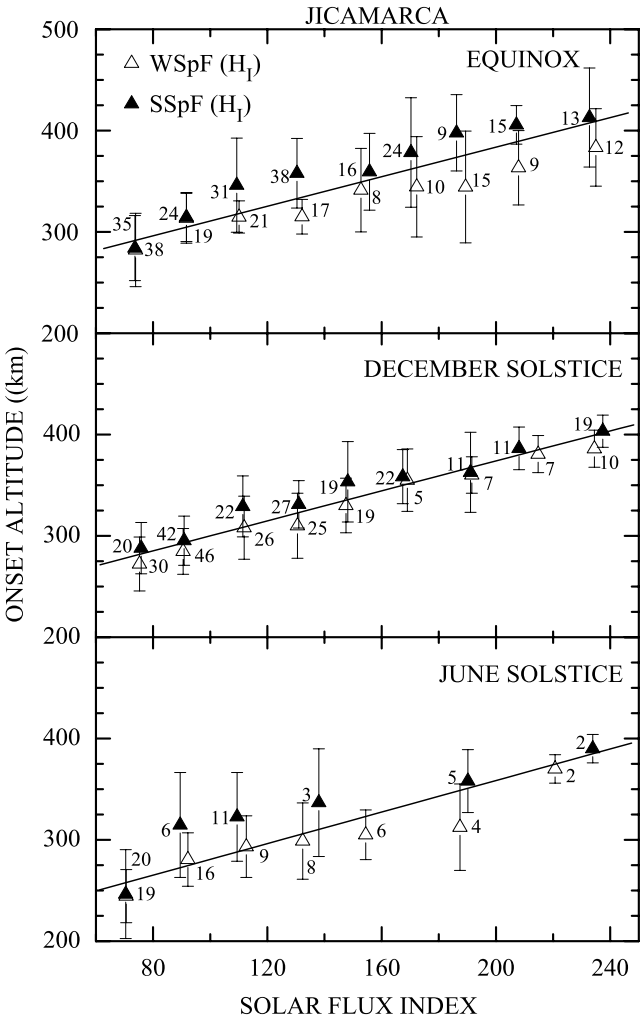

Figure 3. Onset altitudes of weak and strong spread *F* as a function of solar flux index. The number of samples and standard deviations are also shown. The straight lines denote the least squares fit to the combined weak and strong spread *F* data.

ally higher than 160 units, radar plumes often extended above the standard highest height sampled (900 km), which resulted in a smaller database. In the present study, we will consider the characteristics of the initial radar plumes only. When multiplumes are present, their average periods are on the order of 1–1.5 h. *Woodman and LaHoz* [1976] pointed out that the narrow beam (about 1°) of the Jicamarca radar gives only a slit camera view of the irregularities. Therefore the observed times and heights to be discussed below correspond to the values inside the radar beam only.

3. Results

[10] In this section, we will describe the season- and solar flux-dependent onset times and heights of early night spread *F* and radar plumes over Jicamarca, along with their relationships to the evening *F* region vertical drifts.

3.1. Spread *F* Onset Times and Heights

[11] We have initially binned the data on the basis of geomagnetic activity, as indicated by the K_p indices, following the criteria by *Fejer et al.* [1999]. Although spread *F* occurrence is clearly affected by geomagnetic activity, our results indicate that the average characteristic times and heights of spread *F* events are essentially magnetic activity independent. Therefore the results below were obtained by including all available observations, since those improve their statistical significance.

[12] Figure 3 shows the seasonal and solar cycle dependence of the onset heights of weak and strong spread *F* (i. e., broad structures and plumes) obtained by binning the data in groups of 20 solar flux (*F*10.7 cm) units. The linear fits for the average onset heights (H_I) are H_I (km) = 239 + 0.7Φ for the equinox, H_I (km) = 226 + 0.7Φ for the December solstice, and H_I (km) = 203 + 0.8Φ for the June solstice, where Φ is the decimetric solar flux index. These results illustrate the strong increase of the onset heights with solar flux. The average heights vary from about 280 to 420 km in equinox, 270 to 410 km during the December solstice, and 250 to 400 km during the June solstice, as the solar flux index increases from 60 to 250. Near solar minimum, the average onset heights of both weak and strong spread *F* are nearly the same, but for higher solar conditions, the onset heights of strong spread *F* events are generally higher by about 20 km.

[13] Jicamarca ionosonde data (not shown here) show that during spread *F* events, the base of the *F* layer ($h'F$)

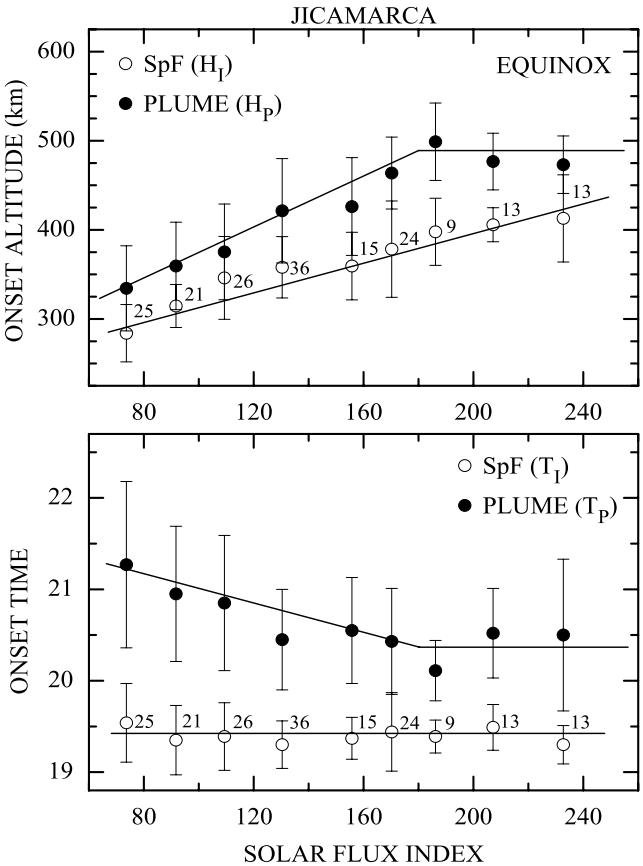

Figure 4. The variations of onset altitudes and times of equatorial spread *F* and resulting radar plumes with solar flux during the equinox. The solid lines denote fits to the data.

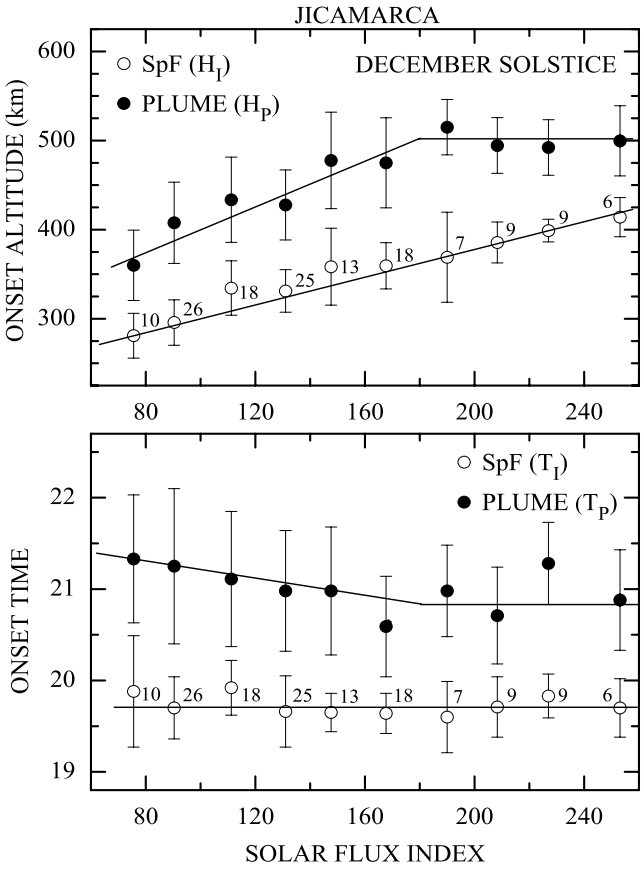

Figure 5. The variations of onset altitudes and times of equatorial spread *F* and radar plumes with solar flux during the December solstice. The solid lines denote fits to the data.

increases from about 290 to 410 km in the equinox, and from 290 to 430 km during the December solstice. These results indicate that, as expected [e.g., *Hysell and Burcham*, 1998; *Kudeki and Bhattacharyya*, 1999], spread *F* occurs initially in the bottomside of the *F* layer.

[14] Figures 4 and 5 present the solar flux variations of spread *F* onset times and heights and resulting radar plumes during the equinox and December solstice. The scatter bars illustrate the large variability of the data. The onset times do not change much with solar flux and have values of about 1920 LT and 1945 LT during the equinox and December solstice, respectively. For moderate and higher solar flux conditions, these onset altitudes are higher than shown in Figure 3, which also include results from weak spread *F*. We do not show the data for the June solstice when, except for solar minimum, spread *F* events are much less frequent over Jicamarca. During the June solstice, spread *F* onset occurs at about 1930 LT, and plume onset times shift from about 2200 to 2030 LT from solar minimum to solar maximum.

[15] Figures 4 and 5 show that plume onset heights over Jicamarca increase from about 330 to 500 km during the equinox and 360 to 500 km during the December solstice from low to moderate solar flux conditions (solar flux index smaller than 180), and then remain nearly unchanged at about 500 km for higher levels of solar activity. Near solar maximum, spread *F* onset times remain nearly unchanged at about 2030 LT in the equinox and 2100 LT during the December solstice. As solar flux increases from low to moderate values, plume onset times shift from about 2115 to 2025 LT in the equinox and from 2120 to 2030 LT during the December solstice. They occur later during January and December than during February and November. This behavior is consistent with the solar cycle dependence of the evening vertical drift velocities [e.g., *Fejer et al.*, 1991].

[16] The average plume onset heights are higher than the corresponding spread *F* onset heights by about 50 to 100 km during the equinox, about 80 to 150 km during the December solstice, and about 30 to 90 km during the June solstice. Near solar minimum, the average time periods from spread *F* onset to plume onset are about 1 h and 45 min in the equinox and about 2 h during the December solstice. For moderate and maximum solar conditions, these periods decrease to about 1 h during the equinox and 1 h and 30 min during the December solstice. Very small numbers of plumes were observed during the June solstice for moderate and high solar flux conditions.

3.2. Plume Peak Heights

[17] Figure 6 shows the scatterplots of the onset and peak heights of the spread *F* plumes over Jicamarca as a function of the solar flux. In this case, the database during moderate

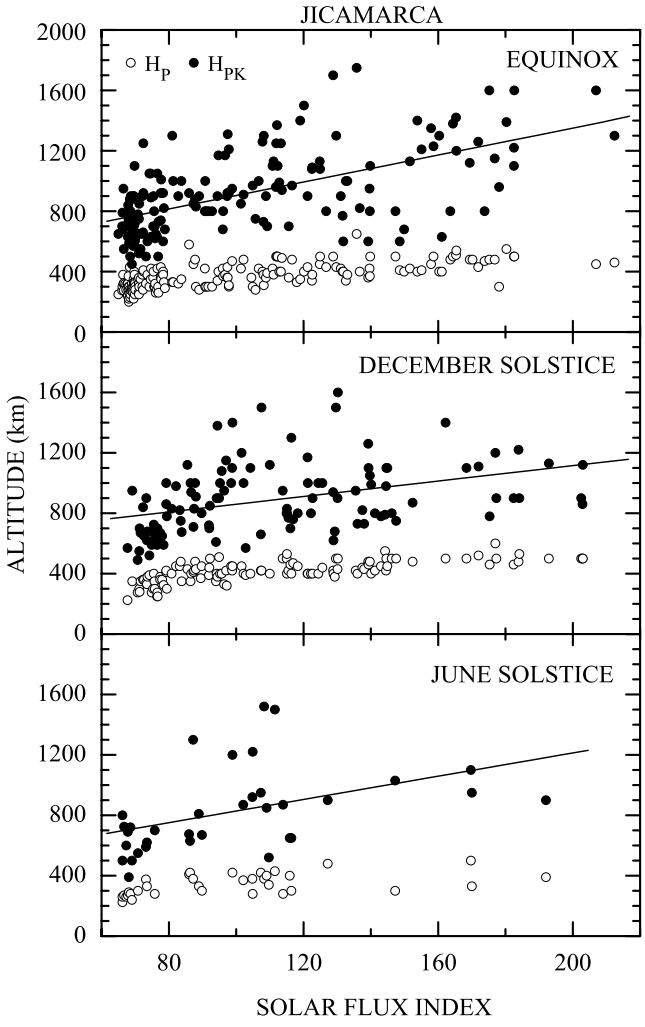

Figure 6. Scatterplots of radar plume onset (H_P) and peak (H_{PK}) heights as a function of solar flux. The straight lines indicate least squares fits to the peak altitude data.

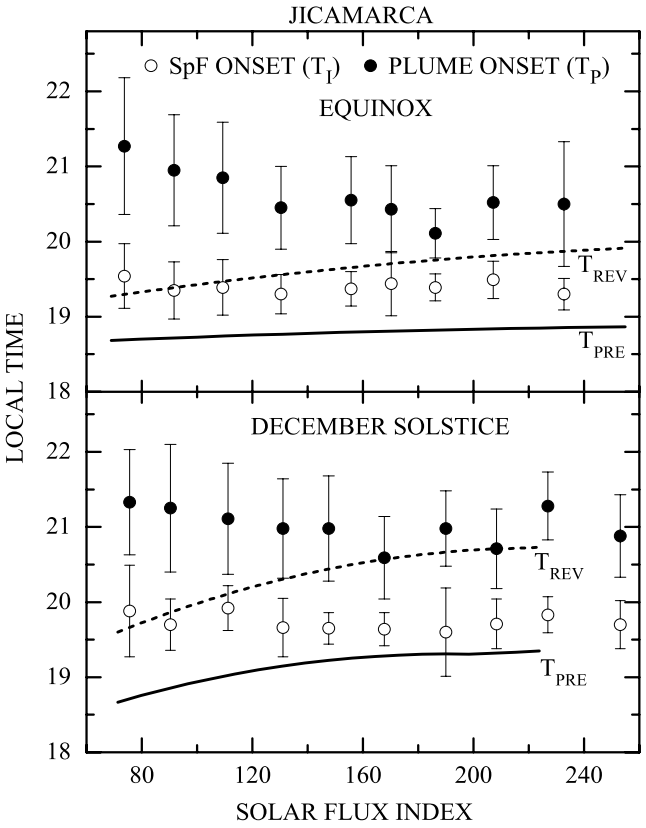

Figure 7. Times of average vertical prereversal drift peaks (solid lines) and drift reversals (dashed lines), spread *F* (T_I), and corresponding radar plume (T_P) onset times as a function of solar flux index.

and high solar flux conditions is much smaller than used in Figures 4 and 5. The onset height, H_p, can be interpreted as corresponding to the altitude that the plume breaks through the top of the *F* layer. Peak height data were not available during January–February high solar conditions. Therefore the December solstice data shown in Figure 6 are mainly from November and December.

[18] Figure 6 illustrates that the peak heights are highly variable but increase significantly from solar minimum to solar maximum. The average plume onset heights increase from about 310 to 500 km as the solar flux index increases from 70 to 200. The peak heights have much larger scatter than the spread *F* onset heights. The equations for the average peak heights are H_{PK}(km) = 472 + 4.3Φ for the equinox, H_{PK}(km) = 604 + 2.6Φ for the December solstice, and H_{PK}(km) = 443 + 3.8Φ for the June solstice. The peak values are about 700 and 1400 km during solar minimum and maximum, respectively. The maximum plume altitude recorded at Jicamarca was about 1800 km during the equinox. The percentages of plumes above 900 km during equinox and December solstice are about 15%, 60%, and 75% for low, moderate, and high solar activity, respectively. During the June solstice, this percentage is about 25% for both low and high solar flux conditions.

3.3. Relationships to Vertical Drift Velocity

[19] Figure 7 illustrates the solar flux dependence of the times of evening drift peak and drift reversal, and spread *F* and plume onset times. As shown in the earlier studies [e.g., *Fejer*, 1991; *Scherliess and Fejer*, 1999], the evening vertical drift peaks and drift reversals occur later in the December solstice than during the equinox, and are latest in January. Since spread *F* onset does not change with solar flux, but the times of drift peak and reversal occur earlier at solar minimum than at solar maximum, the onset times change from near the reversal times to closer to the drift peak times with increasing solar flux. Figure 7 shows that plume onsets over Jicamarca occur about 2 h after the drift reversal during solar minimum, and after about 30 min near solar maximum.

[20] Figure 8 shows the seasonal and solar cycle dependence of the prereversal vertical drift peaks and of the drift velocities preceding the onset of weak spread *F*, and also of spread *F* with subsequent development of radar plumes. The drift velocities were obtained using incoherent scatter radar measurements within ±5 min of spread *F* onset and at the onset height. We should point out that these onset velocities are not necessarily directly related to the observed spread *F* events, since these irregularities could have been generated outside the radar beam. Figure 8 illustrates the large variability of these velocities, particularly during the equinox. Early night downward drifts do not lead to the development of radar plumes during the equinox and inhibit the development of spread *F* during the December solstice. Weak spread *F* can occur even when the local drift velocities near dusk are downward provided that the prereversal peak velocities are positive, which is in good agreement with the results of *Fejer et al.* [1999].

[21] The onset drifts and the corresponding prereversal velocity peaks are generally higher on nights of spread *F*

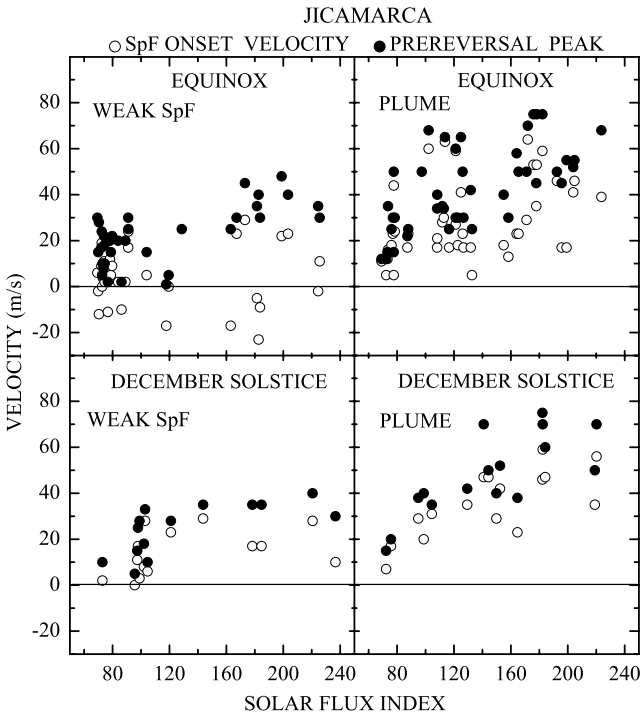

Figure 8. Scatterplots of weak spread *F* and plume onset velocities and corresponding prereversal drift peaks as a function of solar flux index.

plumes. The variability of the onset drifts and prereversal velocity peaks generally decrease with increasing solar activity. We do not present the results for the June solstice when strong spread *F* echoes are rarely seen; only very few of them have been observed with incoherent scatter radar measurements.

4. Discussion

[22] The main results of our observations are:

[23] 1. The spread *F* average onset heights over Jicamarca strongly increase from solar minimum to solar maximum, but their onset times are essentially solar flux independent.

[24] 2. Strong spread *F* events have generally higher onset heights than weak spread *F* for all seasons.

[25] 3. The onset heights of the radar plumes increase with solar flux, but the onset times become earlier from low to moderate solar flux conditions, and remain nearly constant for higher flux values.

[26] 4. The average peak heights of radar plumes increase from about 700 to 1400 km from solar minimum to solar maximum.

[27] 5. Over Jicamarca, spread *F* onsets occur close to the evening drift reversal times during the equinox for all solar flux values. During the December solstice, they occur near drift reversal time near solar minimum, and, for higher solar flux conditions, closer to the time of the prereversal velocity peak.

[28] 6. The spread *F* onset velocities and the prereversal drift peaks are highly variable; these velocities generally determine the equatorial spread *F* signature and echo strength.

[29] The effects of the PRE on the height of the *F* layer and spread *F* onset have been discussed by several authors [e.g., *Farley et al.*, 1970; *Abdu et al.*, 1983; *Sultan*, 1996; *Fejer et al.*, 1999]. *Hysell and Burcham* [2002] used JULIA radar data to show that the height of bottomtype layers typically increase from about 200 to 400 km for an increase in solar flux index from 70 to 200. *Jyoti et al.* [2004] used ground-based ionospheric data from Trivandrum (8.5°N, 76.5°E) and Sriharikota (13.7°N, 80.2°E), India, to show that, the average base heights of the bottomside of the *F* region ($h'F$) at the time of triggering equatorial spread *F* during the equinox increase from about 225 to 350 km with the increase in the solar flux index from about 70 to 120.

[30] *Kudeki and Bhattacharyya* [1999] have shown that bottomside spread *F* commences near the post sunset velocity vortex, which is characterized by upward and downward flows to the west and to the east and eastward and westward flows on the top and the bottom, respectively. They also reported that near solar minimum, this vortex is centered at an altitude of about 250 km. The evening upward drift velocities increase with solar flux moving the base of the equatorial *F* layer and the velocity vortex to higher altitudes. Our spread *F* onset height data suggest that the altitude of the evening vortex reaches up to about 400 km near solar maximum.

[31] We have seen that as solar flux increases the onset heights of spread *F* and plumes occur at higher altitudes and that radar plumes penetrate to higher topside altitudes. *Valladares et al.* [2004] showed a radar plume detected by JULIA extending to a peak height of about 1600 km, and that the corresponding larger-scale scintillations extended up to magnetic latitudes of about 22°. *Tsunoda and Ecklund* [2007] examined the post sunset rise of the equatorial *F* layer and the development of equatorial spread *F* using 50 MHz backscatter radar observations from Pohnpei, Micronesia (7°N, 158.2°E). They reported radar plumes rising to an altitude of about 1400 km. These earlier results are in good agreement with our climatological heights.

[32] Apex height mapping of airglow depletions have shown that altitudes above 2000 km can be reached [e.g., *Kelley et al.*, 2002; *Otsuka et al.*, 2004; *Mendillo et al.*, 2005; *Martinis and Mendillo*, 2007; *Makela and Miller*, 2008]. Recently, *Huba et al.* [2008] reported three-dimensional simulations showing that the bubbles rise from about 400 to 1000 km altitude in roughly one hour, and then to about 1600 km in the next half hour during moderate solar conditions. Our results indicate that the characteristic heights of the 50 MHz scattering layers over Jicamarca are consistent with those from larger-scale spread *F* plasma structures.

[33] We have pointed out that spread *F* onset heights do not change much with geomagnetic activity and that the onset drifts and prereversal velocity enhancements are generally higher on nights of radar plumes. These results further suggest that the major role of geomagnetic activity on equatorial spread *F* results from its effect on the vertical drift velocity, which is consistent with the results of *Fejer et al.* [1999].

5. Conclusions

[34] This paper presents a climatological study of post-sunset equatorial spread *F* over Jicamarca using an extensive data set of coherent and incoherent radar observations. We showed that the onset heights of equatorial spread *F* related to the evening velocity vortex over Jicamarca strongly increase from solar minimum to solar maximum but that the onset times remain nearly unchanged. The onset heights prior to strong spread *F* are generally larger than those of weak spread *F* during moderate and maximum solar conditions. Radar plumes onset shift to later local times from solar minimum to solar moderate conditions and remain constant for high flux values. Plume onset heights increase with solar flux. The peak heights of the radar plumes inside the Jicamarca radar beam are highly variable, but on average, they increase by about 500 km from solar minimum to solar maximum.

[35] The spread *F* onsets during the equinox generally occur close to the reversal times of the vertical drift velocity, when the *F* layer reaches its highest altitude. During the December solstice, these radar echoes first occur near the drift reversal time near solar minimum and closer to the time of the velocity reversal for high solar flux values. The prereversal vertical drift peaks and spread *F* onset drifts are highly variable, and the characteristics of the scattering layer and echo strength are strongly dependent on the values of these velocities.

[36] **Acknowledgments.** The work at Utah State was supported by the Aeronomy program of the National Science Foundation through grant ATM-0534038. The Jicamarca Radio Observatory is a facility of the Instituto Geofisico del Peru and is operated with support from the NSF cooperative agreement ATM-0432565 through Cornell University. The

authors thank the Jicamarca staff for their support, in particular, the members of the radar operations group.

[37] Amitava Bhattacharjee thanks the reviewers for their assistance in evaluating this paper.

References

Abdu, M. A., R. T. Medeiros, J. A. Bittencourt, and I. S. Batista (1983), Vertical ionization drift velocities and range type spread *F* in the evening equatorial ionosphere, *J. Geophys. Res.*, *88*, 399–402.

de Paula, E. R., and D. L. Hysell (2004), The Sao Luis 30 MHz coherent scatter ionospheric radar: System description and initial results, *Radio Sci.*, *39*, RS1014, doi:10.1029/2003RS002914.

Farley, D. T., B. B. Basley, R. F. Woodman, and J. P. McClure (1970), Equatorial spread *F*: Implications of VHF radar observations, *J. Geophys. Res.*, *75*, 7199–7216.

Fejer, B. G. (1991), Low latitude electrodynamic plasma drifts: A review, *J. Atmos. Terr. Phys.*, *53*, 677–693.

Fejer, B. G. (1997), The electrodynamics of the low-latitude ionosphere: Recent results and future challenges, *J. Atmos. Terr. Phys.*, *13*, 1465–1482.

Fejer, B. G., and M. C. Kelley (1980), Ionospheric irregularities, *Rev. Geophys.*, *18*, 401–454.

Fejer, B. G., E. R. de Paula, S. A. Gonzales, and R. F. Woodman (1991), Average vertical and zonal *F* region plasma drifts over Jicamarca, *J. Geophys. Res.*, *96*, 13,901–13,906.

Fejer, B. G., L. Scherliess, and E. R. de Paula (1999), Effect of the vertical plasma drift velocity on the generation and evolution of equatorial spread *F*, *J. Geophys. Res.*, *104*, 19,859–19,869.

Huba, J. D., and G. Joyce (2007), Equatorial spread *F* modeling: Multiple bifurcation structures, secondary instabilities, large density "bite-outs", and supersonic flows, *Geophys. Res. Lett.*, *34*, L07105, doi:10.1029/2006GL028519.

Huba, J. D., G. Joyce, and J. Krall (2008), Three-dimensional equatorial spread *F* modeling, *Geophys. Res. Lett.*, *35*, L10102, doi:10.1029/2008GL033509.

Hysell, D. L. (2000), An overview and synthesis of plasma irregularities in equatorial spread *F*, *J. Atmos. Sol.-Terr. Phys.*, *62*, 1037–1056.

Hysell, D. L., and J. D. Burcham (1998), JULIA radar studies of equatorial spread *F*, *J. Geophys. Res.*, *103*, 29,155–29,167.

Hysell, D. L., and J. D. Burcham (2002), Long term studies of equatorial spread *F* using the JULIA radar at Jicamarca, *J. Atmos. Sol.-Terr. Phys.*, *64*, 1531–1543.

Jayachandran, B., N. Ballan, P. B. Rao, J. H. Sastri, and G. J. Bailey (1993), HF Doppler and ionosonde observations on the onset conditions of equatorial spread *F*, *J. Geophys. Res.*, *98*, 13,741–13,750.

Jyoti, N., C. V. Devasia, R. Sridharan, and D. Tiwari (2004), Threshold height $(h'F)_c$ for the meridional wind to play a deterministic role in the bottom side equatorial spread *F* and its dependence on solar activity, *Geophys. Res. Lett.*, *31*, L12809, doi:10.1029/2004GL019455.

Kelley, M. C. (1989), The Earth's Ionosphere: Plasma physics and electrodynamics, *Int. Geophys. Ser.*, vol. 43, Academic, San Diego, Calif.

Kelley, M. C., J. J. Makela, B. M. Ledvina, and P. M. Kintner (2002), Observations of equatorial spread *F* from Haleakala, Hawaii, *Geophys. Res. Lett.*, *29*(20), 2003, doi:10.1029/2002GL015509.

Kudeki, E., and S. Bhattacharyya (1999), Postsunset vortex in equatorial *F* region plasma drifts and implications for bottomside spread *F*, *J. Geophys. Res.*, *104*, 28,163–28,170.

Kudeki, E., A. Akgiray, M. Milla, J. L. Chau, and D. L. Hysell (2008), Equatorial spread *F* initiation: Post-sunset vortex, thermospheric winds, gravity waves, *J. Atmos. Sol.-Terr. Phys.*, *69*, 2416–2427.

Makela, J. J., and E. S. Miller (2008), Optical observations of the growth and day-to-day variability of equatorial plasma bubbles, *J. Geophys. Res.*, *113*, A03307, doi:10.1029/2007JA012661.

Martinis, C., and M. Mendillo (2007), Equatorial spread *F*-related airglow depletions at Arecibo and conjugate observations, *J. Geophys. Res.*, *112*, A10310, doi:10.1029/2007JA012403.

Mendillo, M., E. Zesta, S. Shodham, P. J. Sultan, R. Doe, Y. Sahai, and J. Baumgardner (2005), Observations and modeling of the coupled latitude-altitude patterns of equatorial plasma depletions, *J. Geophys. Res.*, *110*, A09303, doi:10.1029/2005JA011157.

Otsuka, Y., K. Shiokawa, T. Ogawa, and P. Wilkinson (2004), Geomagnetic conjugate observations of medium-scale traveling ionospheric disturbances at midlatitude using all-sky airglow imagers, *Geophys. Res. Lett.*, *31*, L15803, doi:10.1029/2004GL020262.

Patra, A. K., D. Tiwari, S. Sripathi, P. B. Rao, R. Sridharan, C. V. Devasia, K. S. Viswanathan, K. S. V. Subbarao, R. Sekar, and E. A. Kherani (2005), Simultaneous radar observations of meter-scale *F* region irregularities at and off the magnetic equator over India, *J. Geophys. Res.*, *110*, A02307, doi:10.1029/2004JA010565.

Scherliess, L., and B. G. Fejer (1999), Radar and satellite global equatorial *F* region vertical drift model, *J. Geophys. Res.*, *104*, 6829–6842.

Sultan, P. J. (1996), Linear theory and modeling of the Rayleigh-Taylor instability leading to the occurrence of equatorial spread *F*, *J. Geophys. Res.*, *101*, 26,875–26,891.

Tsunoda, R. T. (2005), On the enigma of day-to-day variability in equatorial spread *F*, *Geophys. Res. Lett.*, *32*, L08103, doi:10.1029/2005GL022512.

Tsunoda, R. T., and W. L. Ecklund (2007), On the post-sunset rise of the equatorial *F* layer and superposed upwellings and bubbles, *Geophys. Res. Lett.*, *34*, L04101, doi:10.1029/2006GL028832.

Valladares, C. E., R. Sheehan, and J. Villalobos (2004), A latitudinal network of GPS receivers dedicated to studies of equatorial spread *F*, *Radio Sci.*, *39*, RS1S23, doi:10.1029/2002RS002853.

Woodman, R. F., and C. LaHoz (1976), Radar observations of *F* region equatorial irregularities, *J. Geophys. Res.*, *81*, 5447–5466.

Yokoyama, T., S. Fuko, and M. Yamamoto (2004), Relationship of the onset of equatorial *F* region irregularities with the sunset terminator observed with the Equatorial Atmosphere Radar, *Geophys. Res. Lett.*, *31*, L24804, doi:10.1029/2004GL021529.

J. L. Chau, Radio Observatorio de Jicamarca, Instituto Geofisico del Peru, Apartado 13-0207, Lima 13, Peru.

N. P. Chapagain and B. G. Fejer, Center for Atmospheric and Space Sciences, Utah State University, 246 SER Building, 4405 Old Main Building, Logan, UT 84322-4405, USA. (bela.fejer@usu.edu)